Computational Study of the Ion−Molecule Reactions Involving Fluxional Cations: $CH_4^+ + H_2 \rightarrow CH_5^+ + H$ and Isotope Effect

Baoshan Wang* and Hua Hou

College of Chemistry and Molecular Sciences, Wuhan University, Wuhan 430072, People's Republic of China

Received: July 8, 2005; In Final Form: August 7, 2005

Potential energy surfaces for the reactions of CH_4^+ with H_2, HD, and D_2 have been calculated using high-level ab initio methods, including coupled cluster theory, complete active space self-consistent field, and multireference configuration interaction. The energies are extrapolated to the complete basis set limit using the basis sets aug-cc-pVXZ (X = D, T, Q, 5, 6). The $CH_4^+ + H_2$ reaction produces CH_5^+ and H exclusively. Three types of reaction mechanisms have been found, namely, complex-forming abstraction, scrambling, and S_N2 displacement. The abstraction occurs via a very minor barrier and it is dominant. The other two mechanisms are negligible because of the significant barriers involved. Quantum phase space theory and variational transition state theory are used to calculate the rate coefficients as a function of temperatures in the range of 5−1000 K. The theoretical rate coefficients are compared with the available experimental data and the discrepancy is discussed. The significance of isotope effect, tunneling effect, and nuclear spin effect is investigated. The title reaction is predicted to be slightly exothermic with $\Delta H_r = -12.7 \pm 5.2$ kJ/mol at 0 K.

I. Introduction

The methane cation (CH_4^+) and protonated methane (CH_5^+) are the so-called fluxional species; in other words, they are extremely floppy molecules in which many isoenergetic structures exist due to the nearly free scrambling motion of hydrogen atoms. Previous experimental and theoretical studies[1−16] suggested that the global minimum of CH_4^+ has C_{2v} symmetry with a three-membered ring CH_2 whereas that of CH_5^+ has C_s symmetry with a CH_3 tripod and a 3-center, 2-electron CH_2 structure. In addition, the CH_5^+ ion is the simplest hypercoordinated carbocation. The reactions involving such fluxional ions are very interesting. In this paper we present the first theoretical study on the reaction:

$$CH_4^+ + H_2 \rightarrow CH_5^+ + H \quad (1)$$

Deuterated variants of CH_x^+ ($x = 4-6$) are very interesting as well. The replacement of the proton, a fermion, by a deuteron, a boson, reduces the exchange symmetry. Moreover, it changes the zero-point energy and thus changes the reaction paths, viz.:

$$CH_4^+ + HD \rightarrow CH_5^+ + D \quad (2a)$$

$$\rightarrow CH_4D^+ + H \quad (2b)$$

$$\rightarrow CH_3D^+ + H_2 \quad (2c)$$

and

$$CH_4^+ + D_2 \rightarrow CH_4D^+ + D \quad (3a)$$

$$\rightarrow CH_3^+D + HD \quad (3b)$$

$$\rightarrow CH_2D_2^+ + H_2 \quad (3c)$$

The $CH_4^+ + H_2 \rightarrow CH_5^+ + H$ reaction is an important chemical process in low-density interstellar clouds. Several decades ago Munson et al. observed the interaction between CH_4^+ and H_2 using a mass spectrometer.[17] The absolute rate coefficient was first measured by Kim et al. in a 300 K ion-cyclotron resonance apparatus ($k_1 = 4.1 \times 10^{-11}$ cm^3/s).[18] Adams and Smith performed a room-temperature measurement using a selected ion flow tube (SIFT, $k_1 = 3.3 \times 10^{-11}$ cm^3/s).[19] The first dedicated energy-dependent measurement of k_1 was reported by Federer et al. using a selected ion flow drift tube (SIFDT).[20] They found that the rate coefficients decrease with increasing energy between 40 and 120 meV.

The most comprehensive experimental studies of $CH_4^+ + H_2$ were carried out very recently by Asvany, Savic, Schlemmer, and Gerlich (ASSG) using a variable temperature 22-pole ion trap from room temperature down to 15 K.[21] The reaction is slow at 300 K with $k_1 = 3.3 \times 10^{-11}$ cm^3/s, but it becomes faster by more than 1 order of magnitude when the temperature is lowered to 15 K with $k_1 = 4.0 \times 10^{-10}$ cm^3/s. In addition, the isotope effect was also studied by ASSG. A negative temperature dependence of the rate coefficients was observed for the collisions of CH_4^+ with HD and D_2. The reaction of CH_4^+ with HD is as fast as with H_2. However, the $CH_4^+ + D_2$ reaction was found to be much slower. More interestingly, the CH_5^+ product ion in channel (2a) prevails over CH_4D^+ in channel (2b), although the latter is energetically more favorable.

Although the kinetic behavior of the $CH_4^+ + H_2$ reaction has been studied extensively, the reaction mechanism is unknown. Less is known for the possible reaction complex CH_6^+, which is also a hypercoordinated cation. In this work four questions will be addressed:

First, what is the reaction mechanism? Although it is an isoelectronic reaction with the well-known $NH_3^+ + H_2 \rightarrow NH_4^+ + H$ reaction, the $CH_4^+ + H_2$ reaction occurs via a very different mechanism due to the fluxional nature of reactants and products. Moreover, the reaction involves the hypercoordinated CH_6^+ intermediates. It is interesting to know how CH_6^+ is bonded and if CH_6^+ is as fluxional as CH_4^+ and CH_5^+.

* Corresponding author. E-mail: wangb@chem.whu.edu.cn. Fax: 862768754067.

10.1021/jp053759b CCC: $30.25
Published on Web 09/03/2005

Second, how does the reaction behave at extremely low temperatures? Experimentally, it has been found that the title reaction shows negative temperature dependence in the range 15−1000 K. Variational transition state theory (VTST) with tunneling corrections has been employed to simulate the reaction kinetics. Note that the reactant, H_2, needs special treatment. The normal-H_2 used in the experiments consists of 75% ortho-H_2 (with only odd J) and 25% para-H_2 (with only even J).

Third, how does the isotope affect the reaction mechanism and kinetics? Isotope substitution not only changes the stability of species involved in the reaction but also changes the reaction paths and of course the kinetics. As mentioned above, the strange isotope effect due to HD and D_2 in the title reaction has been found by ASSG and is waiting for explanation from theoretical viewpoint.[21]

Fourth, is the $CH_4^+ + H_2 \rightarrow CH_5^+ + H$ reaction exothermic, endothermic, or thermal-neutral? The heat of reaction is critically important to understand the reverse process. The H atom was thought to be an ideal chemical sensor for laser probing of ultracold CH_5^+. Federer et al. reported that, at room temperature, the destruction of CH_5^+ by H is almost 10 times faster than formation via the $CH_4^+ + H_2$.[20] However, the $CH_5^+ + H \rightarrow CH_4^+ + H_2$ reaction is endothermic by about 19 kJ/mol according to the heats of formation of reactants and products at 0 K,[22] which implies that it is slower than the title reaction. Obviously, an accurate heat of reaction has to be known to rationalize the experimental findings.

The paper is arranged as follows: An overview of the computational methods is given in section II. The reaction mechanisms and the isotopic effect are discussed in section III.1. The comparisons between ab initio mechanisms are made in section III.2. The kinetic simulations are presented in section III.3. The heat of reaction is evaluated in section III.4. A few concluding remarks are drawn in section IV.

II. Computational Details

Two types of ab initio methods have been used to calculate the potential energy surface of the title reaction. The first is coupled cluster theory[23] with single, double, and noniterative triple excitations [CCSD(T)] with the extrapolation to complete basis set (CBS) limit. The restricted scheme using the restricted open-shell Hartree−Fock (ROHF) references, denoted as RCCSD(T),[24] was used to calculate the correlation energies. The basis sets used in the extrapolation include Dunning's correlation-consistent aug-cc-pvdz (AVDZ), aug-cc-pvtz (AVTZ), and aug-cc-pvqz (AVQZ).[25] Three ROHF energies were then extrapolated with the formula advocated by Feller,[26] $E_{HF}^X = E_{HF}^\infty + ae^{-bX}$, where E_{HF}^X is the ROHF energy obtained with the aug-cc-pVXZ basis set. The parameters a and b and the extrapolated ROHF energy E_{HF}^∞ are determined uniquely from the three energies. For the correlation energy, a formula motivated by the atomic partial wave expansion was used, viz.[27] $\Delta E_{RCCSD(T)}^X = \Delta E_{RCCSD(T)}^\infty + c/(X - 1/4)^3$, where $\Delta E_{RCCSD(T)}^X$ is the RCCSD(T) correlation energy (not the total RCCSD(T) energy, which includes the ROHF contribution) obtained with the aug-cc-pVXZ basis set. Here, there are two parameters, c and the estimated complete basis set limit RCCSD(T) correlation energy $\Delta E_{RCCSD(T)}^\infty$. These are uniquely determined by two correlation energies; AVTZ and AVQZ were used in this work.

The geometries of reactants, products, intermediates (IM), and transition states (TS) have been optimized at the CCSD/6-311++G(2d,2p) level of theory. The convergence criteria requires the maximum component of the gradient to be less than 4.5×10^{-4} au and the root-mean-square (RMS) of the gradient to be less than 3×10^{-4} au as well as the maximum component of the optimization step to be less than 1.8×10^{-3} au and the RMS of the optimization step to be less than 1.2×10^{-3} au. Harmonic vibrational frequencies were calculated at the same level to characterize the nature of stationary points and to calculate the zero-point energy (ZPE). The minima have real frequencies and TS has only one imaginary frequency. Another cheaper method, namely, MP2/6-311++G(2d,2p), was used to calculate the minimum energy reaction path (MREP) using the intrinsic reaction coordinate (IRC) method[28] based on the optimized geometries at the same level of theory. Another calculation at the MP2/6-311++G(3df,3pd) level was used to check the effect of the size of the basis sets.

As for the reactants and products, more extensive calculations have been performed. The geometries were re-optimized at the RCCSD(T)/AVTZ level and the harmonic ZPEs were obtained at the same level. Furthermore, the RCCSD(T)/AVQZ optimized geometries were used to calculate the single-point energies at the RCCSD(T) level with aug-cc-pv5z (AV5Z) and aug-cc-pv6z (AV6Z) basis sets, respectively. The RCCSD(T)/CBS energy was obtained using the similar formula as above (E_{HF}^∞ was calculated using ROHF energies at AVQZ, AV5Z, and AV6Z basis sets; $\Delta E_{RCCSD(T)}^\infty$ was calculated using the $\Delta E_{RCCSD(T)}^X$ values at AVQZ and AV5Z levels). In addition, some minor corrections to the total energies were calculated on the basis of the RCCSD(T)/AVQZ optimized geometries, including the scalar relativistic effects, diagonal Born−Oppenheimer correction (DBOC), and spin−orbit (SO) correction.[29−31] The details will be given in section III.4. It should be noted that the couple cluster calculations include *all* electrons in the electron correlation evaluations.

The second ab initio method is the multireference configuration interaction with single and double excitations (MRCISD).[32] The geometries of the critical stationary points were optimized using the complete active space self-consistent-field (CASSCF) method[33] with the AVTZ and AVQZ basis sets. Supermolecule approximation was used to deal with reactants and products. The active space includes all valence electrons and all valence orbitals [e.g., 9 electrons in 10 orbitals]. The harmonic vibrational frequencies were calculated at the CASSCF/AVTZ level. Subsequently, the energies of various stationary points were calculated using MRCISD with the CASSCF generated reference configurations. Three CASSCF energies (AVTZ, AVQZ, and AV5Z) and two MRCISD correlation energies (AVQZ and AV5Z) were used for the CBS limit extrapolation according to the formula:[34] $E_{HF}^X = E_{HF}^\infty + ae^{-bX}$ and $\Delta E_{MRCI}^X = \Delta E_{MRCI}^\infty + c/X^3$. The Davidson correction (e.g., MRCISD+Q or simply, Full CI) was used to estimate the correlations from higher excitations. The same fashion of CBS extrapolation was used to obtain the MRCISD+Q energies.

It is worth mentioning the sizes of the basis sets and the reference configurations spaces. The numbers of contracted basis functions are 184, 356, and 607 for AVTZ, AVQZ, and AV5Z, respectively. The largest basis set used in this work, AV6Z, consists of 824 contractions. With the AV5Z basis set, each CASSCF job consists of 27 720 configuration state functions (CSFs) and each MRCISD job includes 19 332 092 contracted configurations obtained from 3 291 779 512 uncontracted configurations.

The rate coefficients of the title reactions were calculated using the multichannel RRKM theory and transition state theory. Quantum phase space theory (QPST)[35] and rigid rotor harmonic oscillator (RRHO) were employed to deal with the barrierless

a

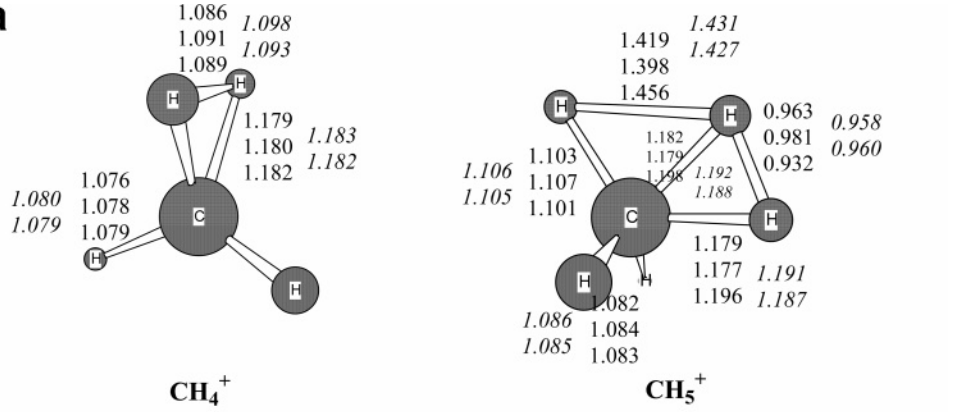

CH_4^+ CH_5^+

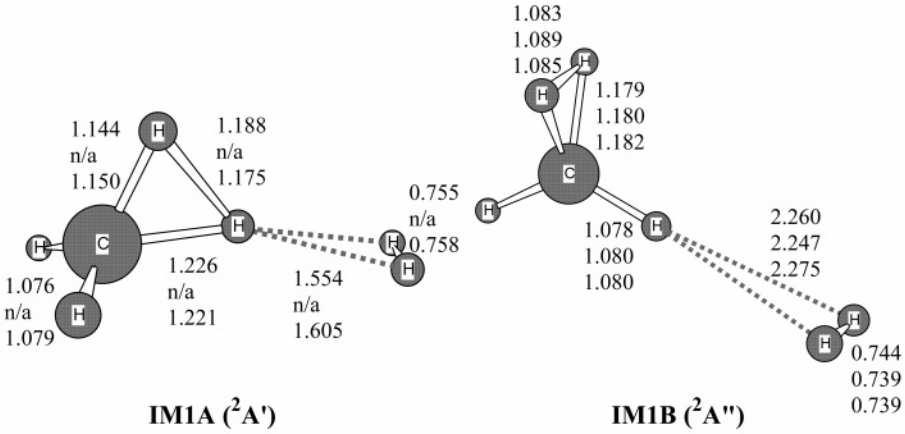

IM1A (^{2}A') IM1B (^{2}A")

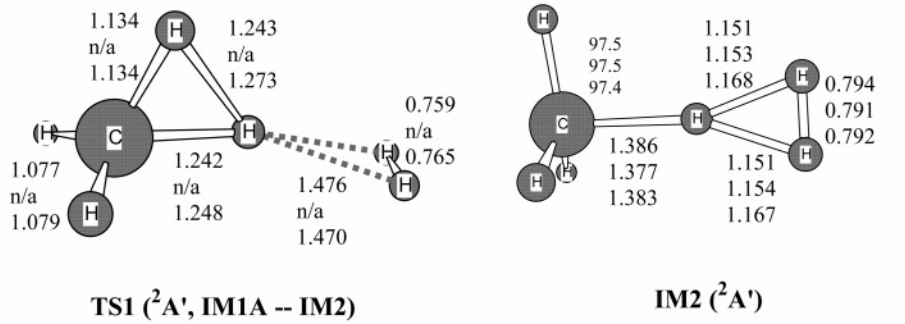

TS1 (^{2}A', IM1A -- IM2) IM2 (^{2}A')

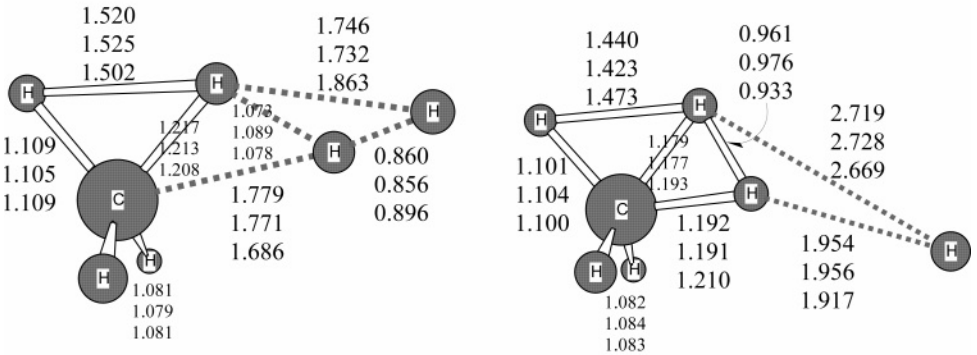

TS2 (^{2}A', IM2 -- IM3A) IM3A (^{2}A')

b

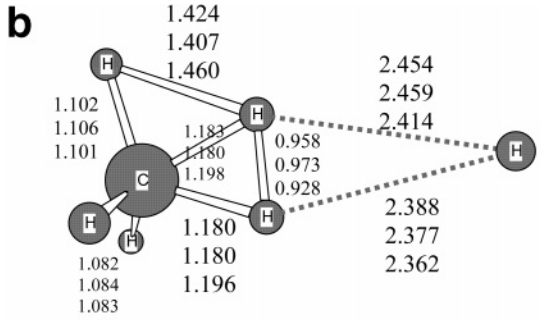

TS3 (^{2}A', IM3A -- IM3B)

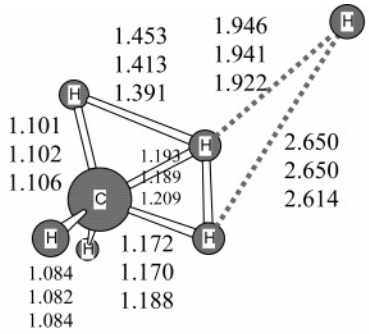

IM3B (^{2}A')

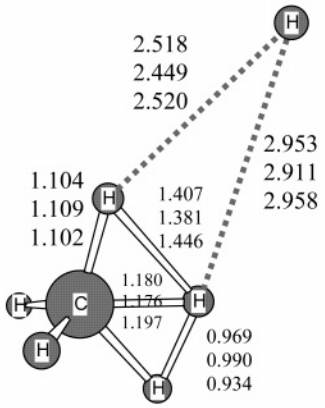

TS4 (^{2}A', IM3B -- IM3C)

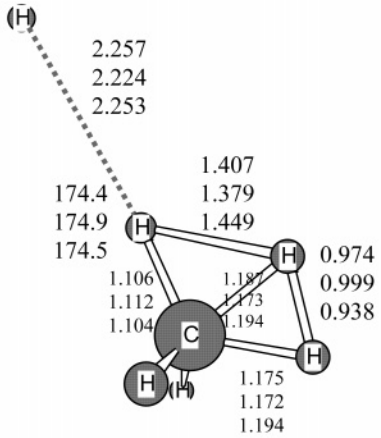

IM3C (^{2}A')

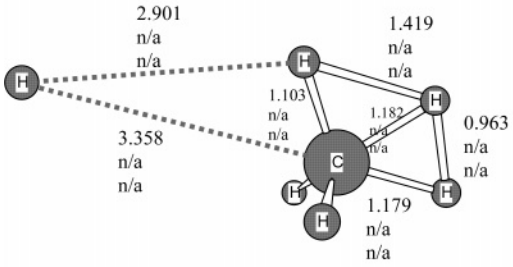

TS5 (^{2}A', IM3C -- IM3D)

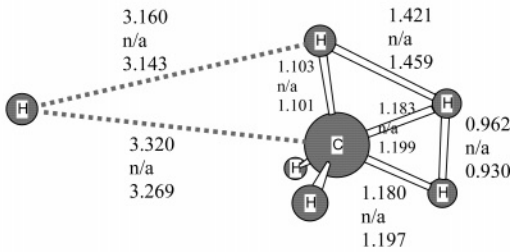

IM3D (^{2}A')

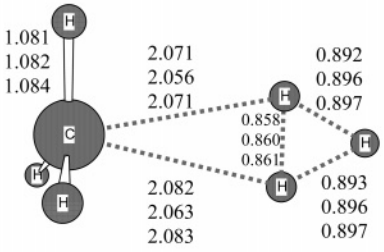

TS6 (scrambling, ^{2}A')

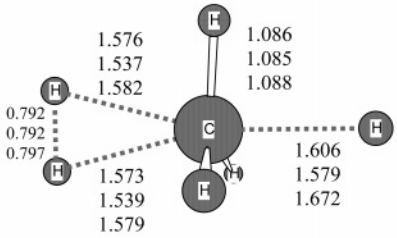

TS7 (S_N2, ^{2}A')

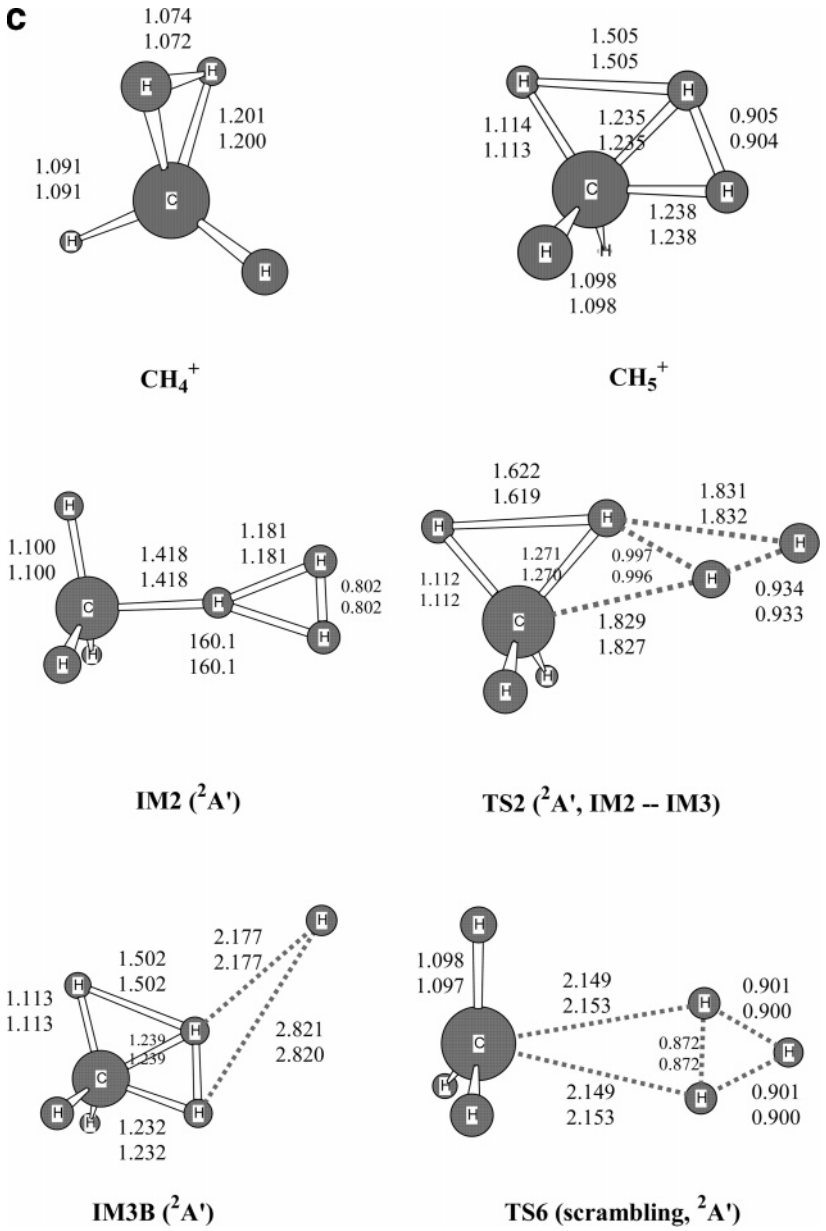

Figure 1. Optimized geometrical parameters for various species involved in the $CH_4^+ + H_2$ reaction (a) for the abstraction mechanism and (b) for the scrambling and S_N2 mechanisms. Bond distances are in Å. From top to bottom, three entries correspond to MP2/6-311++G(2d,2p), MP2/6-311++G(3df,3pd), and CCSD/6-311++G(2d,2p) data, respectively. n/a: not available. For CH_4^+ and CH_5^+, the two entries in italics are the optimized parameters at the RCCSD(T) level with AVTZ (upper) and AVQZ (lower) basis sets, respectively. (c) The CASSCF/AVTZ (upper) and CASSCF/AVQZ (lower) optimized parameters.

channels and the tight transition state, respectively. The details will be given in section III.3.

The CCSD and MP2 optimizations were carried out using the Gaussian03 program.[36] All the other ab initio calculations were performed using the Molpro program.[37] PSI program[38] was employed to calculate the DBOC. The kinetic calculations were performed using a modified Variflex code.[39]

III. Results and Discussion

The CCSD and CASSCF optimized structures of the species involved in the $CH_4^+ + H_2 \rightarrow CH_5^+ + H$ reaction are shown in Figure 1a−c, respectively. The schematic profiles of the potential energy surfaces are shown in Figures 2 and 3 (for isotope HD and D_2 reactions 2 and 3). Correspondingly, the calculated rate coefficients as a function of temperature are shown in Figures 4 and 5. The yield of CH_5^+ for the $CH_4^+ +$ HD reaction is shown in Figure 6.

The coupled cluster based relative energies of various species are listed in Table 1, including ZPEs. Table 2 gives the MRCISD/CBS energetic data. The vibrational frequencies calculated at the CCSD/6-311++G(2d,2p) level and the CASSCF/AVTZ level are listed in Tables 3 and 4, respectively. Table 5 summarizes the calculated heats of reaction at various levels of theory. In the following discussion, the coupled cluster data will be used. The MRCISD data will be discussed for purposes of comparison.

1. Reaction Mechanism. The structures of CH_4^+ and CH_5^+ are discussed first. As shown in Figure 1, the lowest energy structure of CH_4^+ is in C_{2v} symmetry with a three-center CH_2 bonding geometry, in which CH and HH bonds are 1.18 and 1.09 Å, respectively. The global minimum of CH_5^+ is of C_s symmetry. It involves a tripod formed by three CH bonds, where two of them are symmetrical and the third is in the plane, and a 3-center, 2-electron CH_2 group, where CH and HH bond

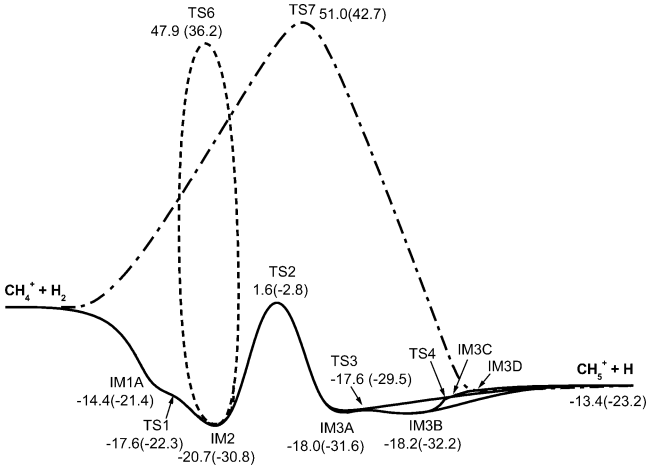

Figure 2. Schematic profile for the potential energy surface of the $CH_4^+ + H_2$ reaction. The energies (kJ/mol) are at the RCCSD(T)/CBS level. The numbers in brackets correspond to the energies without ZPE corrections.

TABLE 1: Relative Energies of Various Species Involved in the $CH_4^+ + H_2$ Reaction on the Basis of the CCSD/6-311++G(2d,2p) Optimized Geometries and ZPEs[a]

species	ZPE	CCSD	G3MP2	RCCSD(T)/CBS[b]
$CH_4^+ + H_2$	127.5	0	0	0
IM1A	134.5	−10.7	−11.2	−14.4
IM1B	132.0	−0.8	−0.9	−1.5
TS1 (IM1A → IM2)	132.1	−12.9	−13.4	−17.6
IM2	137.5	−15.9	−15.0	−20.7
TS2 (IM2 → IM3A)	131.9	10.7	8.0	1.6
IM3A	141.2	−7.3	−13.5	−18.0
TS3 (IM3A → IM3B)	139.4	−6.4	−12.8	−17.6
IM3B	141.5	−7.4	−13.7	−18.2
TS4 (IM3B → IM3C)	138.9	−4.9	−11.4	−15.7
IM3C	139.7	−4.6	−11.1	−15.0
IM3D	138.9	−4.2	−10.6	−14.4
TS6 (scrambling)	139.1	53.9	53.2	47.9
TS7 (S_N2 displacement)	135.8	59.6	57.3	51.0
$CH_5^+ + H$	137.3	−3.9	−4.1	−13.4

[a] All energies are in kJ/mol. [b] The ZPE corrected energies calculated using the RCCSD(T) theory with the extrapolation to complete basis set. See text for details.

distances are 1.18 and 0.93 Å, respectively. The present structural parameters of CH_4^+ and CH_5^+ are in good agreement with previous calculations and experiments.[1−16] The other isoenergetic fluxional structures have been well studied in the literature[1−16] and will not be discussed further.

Mechanistically, there are three different pathways for the $CH_4^+ + H_2$ reaction, namely, abstraction, scrambling, and S_N2-type displacement, as shown in Figure 2. For all the mechanisms, CH_5^+ and H are the only products of the $CH_4^+ + H_2$ reaction at normal conditions. Neither charge-transfer channel ($CH_4 + H_2^+$, $\Delta H_r^0 = 272$ kJ/mol) nor the $CH_3 + H_3^+$ channel ($\Delta H_r^0 = 109$ kJ/mol) is important in view of their endothermicities (estimated using the G3MP2 theory).

The abstraction reaction takes place with the formation of a complex IM1A (see Figure 1). H_2 approaches one of the H atoms of the 3-center CH_2 group of CH_4^+, where one of the CH bonds is stretched slightly and the other CH bond becomes shorter and the HH bond is elongated by about 0.1 Å. The bonding distance between CH_4^+ and H_2 is as short as 1.6 Å. This complex-forming process occurs without passing any barrier. The energy of IM1A is lower than that of the reactants by 14.4 kJ/mol. However, IM1A is not stable because it can readily isomerize to another complex (IM2) via TS1. As shown in Table 1, the energy of TS1 is lower than that of IM1A. It implies that the isomerization from IM1A to IM2 is barrierless. The isomerization occurs by moving H_2 slightly closer toward CH_4^+. The 3-center CH_2 structure of CH_4^+ is broken, and simultaneously, a new 3-center H_3 bonding structure is formed in IM2. In fact, at the MP2 level with the 6-311++G(3df,3pd) basis set, both IM1A and TS1 disappear. Therefore, it is concluded that IM2 is the direct product of the association of CH_4^+ with H_2.

It is noted that the other complex IM1B is formed when H_2 approaches the other end of CH_4^+. The separation between the two fragments is significantly long (ca. 2.2 Å), indicating a very weak interaction. In fact, IM1B belongs to the $^2A''$ electronic state and it is negligible.

The intermediate IM2 is a stable CH_6^+ ion. Its energy is 20.7 kJ/mol below that of the initial reactants. It looks like a $H_3C\cdot H\cdot H_2$ complex. The CH_3 group is nearly planar. The long C·H

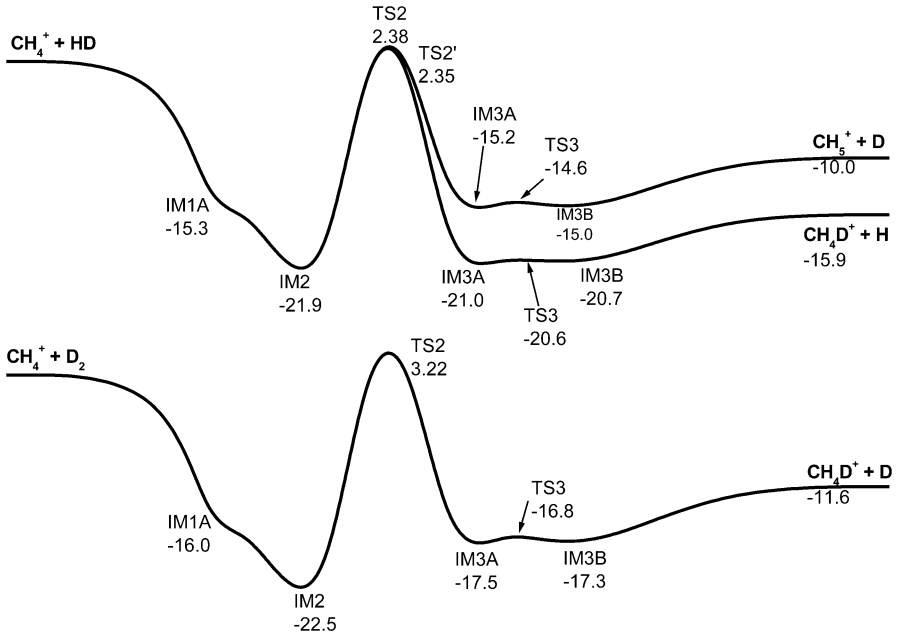

Figure 3. Energy profile for the $CH_4^+ + HD$ (upper panel) and $CH_4^+ + D_2$ (lower panel) reactions. The energies are at the RCCSD(T)/CBS level.

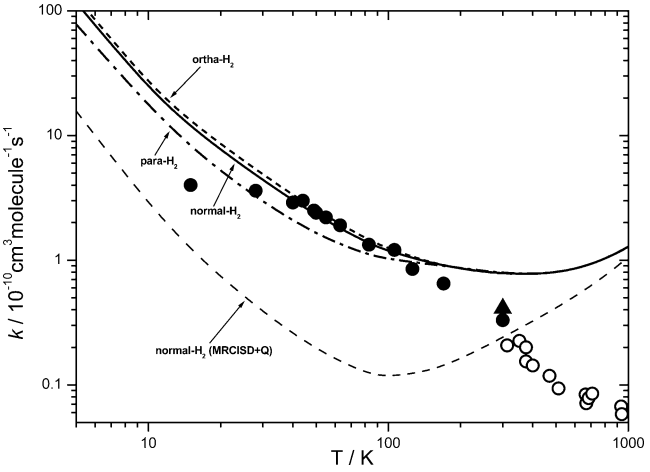

Figure 4. Calculated rate coefficients for the $CH_4^+ + H_2$ reaction: (●) ref 21 (ASSG's experiments); (▲) ref 18 (Kim's experiment); (○) ref 20 (Federer's experiments); (—) normal-H_2 (75% ortho-H_2 plus 25% para-H_2); (---) ortho-H_2; (—·—) para-H_2.

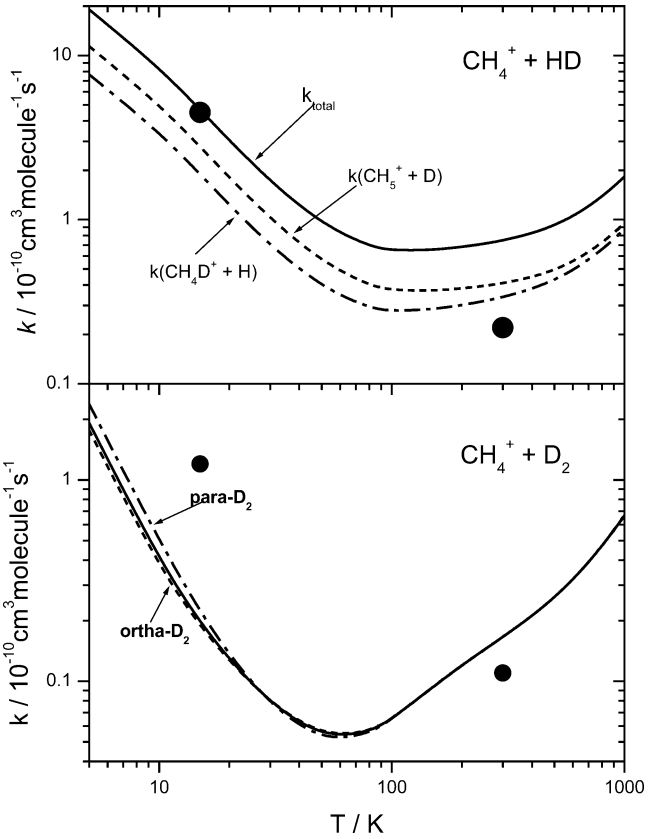

Figure 5. Rate coefficients for the $CH_4^+ + HD$ (upper panel)/D_2 (lower panel) reactions: (—) overall rate coefficients; (●) ref 21 (ASSG's experimental data for the overall rate coefficients).

bond is nearly perpendicular to the CH_3 group. The HH distance in the H_2 group is 0.8 Å, slightly longer than the equilibrium distance of H_2 molecule. The other two H·H bonds are equal (1.15 Å). The most interesting structural characteristic of IM2 is that the C·H bond connecting CH_3 and H_2 is relatively long (1.38 Å). As a result, both CH_3 and H_2 groups in IM2 can rotate freely around this C·H bond, as indicated by its small torsion vibrational frequency (see Tables 3 and 4).

The abstraction continues via TS2. As can be seen in Figure 1, the geometric changes from IM2 to TS2 are very interesting. One of H atoms of the H_2 group moves toward the central C atom by pushing back the central H atom, and two new CH and HH bonds are forming. Simultaneously, the other H atom is moving away from C atom and tending to break the HH bond. As a result, the long CH bond in IM2 is shortened to 1.21 Å; the forming CH and HH bonds are 1.77 and 1.1 Å; the breaking HH bond is stretched to 0.86 Å. Through IRC calculation, it is confirmed that TS2 connects IM2 and IM3A, where the latter corresponds to a complex between the final products CH_5^+ and H atom. Without ZPE, the energy of TS2 is lower than that of the reactants by 2.8 kJ/mol. After ZPE correction, TS2 lies slightly above the reactants by 1.6 kJ/mol.

The energy of IM3A is very close to that of IM2. However, IM3A is less stable than IM2 because it can decompose easily to form the final products $CH_5^+ + H$. The decomposition is endothermic by only 5.4 kJ/mol without additional barrier. As can be seen in Figure 1, the bonding between CH_5^+ and H in IM3A is fairly weak. The nearest HH bond distance is as long as 1.92 Å.

It is interesting to note that IM3A has a few isoenergetic conformations via the following transformation: IM3A → TS3 → IM3B → TS4 → IM3C → TS5 → IM3D → IM3A. Among them, IM3B is the global minimum of the CH_5^+·H complexes. As can be seen from Figure 1, all these conformations are in C_s symmetry. Four H atoms are in the plane and the other two H atoms are symmetrical about the plane. Interestingly, the interconversion between IM3A−D undergoes via H atom circling in an orbital around the central C atom in the symmetry plane of CH_5^+. The barriers for interconversion are so low that the H atom motion is nearly free. This indicates that IM3, which is a CH_6^+ species, is a fluxional ion similar to CH_5^+.

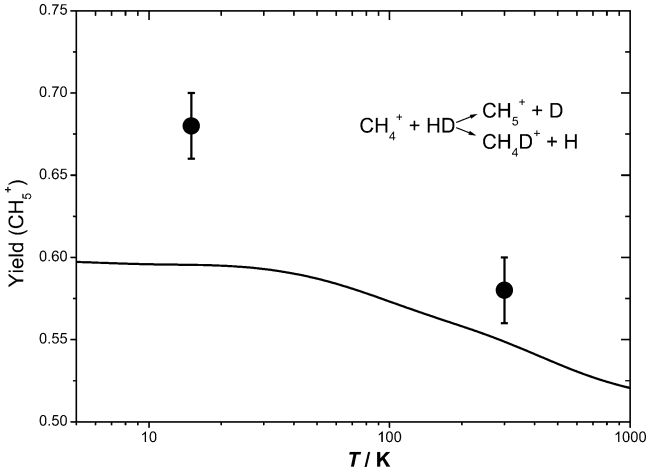

Figure 6. Yields of CH_5^+ in the $CH_4^+ + HD$ reaction: (—) this work; (●) ref 21 (ASSG's experimental data).

TABLE 2: ZPE (kJ/mol), Relative Energies Δ*E* (kJ/mol), and Total Energies *E* (Hartrees) for the Key Species in the $CH_4^+ + H_2$ Reaction at the MRCISD/CBS Level of Theory

species	ZPE[a]	E_{MRCISD}[b]	ΔE_{MRCISD}[c]	E_{FullCI}[d]	ΔE_{FullCI}[e]
$CH_4^+ + H_2$	125.7	−41.155481	0	−41.162618	0
IM2	134.6	−41.155262	−19.4	−41.173404	−19.4
TS2	128.0	−41.154593	4.6	−41.161547	5.1
IM3B	137.8	−41.166534	−17.0	−41.172284	−13.3
TS6	136.1	−41.140712	49.1	−41.169161	49.0
$CH_5^+ + H$	134.7	−41.163561	−12.3	−41.147875	−8.2

[a] Harmonic ZPEs are calculated at the CASSCF/AVTZ level of theory. [b] The total energy at the MRCISD level with the complete basis set limit. [c] The relative energy with respect to $CH_4^+ + H_2$ at the MRCISD /CBS level of theory with ZPE corrections. [d] The estimated Full CI total energies using the MRCISD+Q energies. [e] The estimated relative energy with respect to the $CH_4^+ + H_2$ at the Full CI /CBS level of theory with ZPE corrections. See text for the definition of CBS.

TABLE 3: Harmonic Vibrational Frequencies at the CCSD/6-311++G(2d,2p) Level[a]

species	frequencies (cm^{-1})
$CH_4^+ + H_2$	497, 906, 1192, 1325, 1588, 2301, 2577, 3183, 3326, 4415
IM1A	89, 236, 267, 420, 604, 765, 868, 1044, 1343, 1518, 1970, 2677, 3187, 3318, 4186
IM1B	38, 80, 122, 194, 375, 486, 916, 1197, 1328, 1594, 2300, 2573, 3172, 3318, 4378
TS1 (IM1A → IM2)	352*i*, 82, 304, 444, 619, 750, 842, 1051, 1348, 1486, 1811, 2770, 3186, 3305, 4092
IM2	5, 399, 405, 575, 768, 814, 1163, 1189, 1428, 1429, 1502, 3061, 3230, 3233, 3789
TS2 (IM2 → IM3A)	416*i*, 120, 603, 674, 796, 1091, 1151, 1209, 1352, 1470, 1953, 2226, 2946, 3189, 3276
IM3A	30, 195, 324, 326, 958, 1299, 1310, 1486, 1515, 1638, 2322, 2740, 3050, 3161, 3249
TS3 (IM3A → IM3B)	153*i*, 86, 158, 250, 924, 1310, 1317, 1486, 1514, 1646, 2370, 2790, 3054, 3158, 3249
IM3B	89, 231, 327, 345, 894, 1313, 1322, 1485, 1514, 1633, 2314, 2730, 3052, 3157, 3248
TS4 (IM3B → IM3C)	101*i*, 58, 176, 227, 885, 1311, 1316, 1486, 1512, 1624, 2414, 2765, 3041, 3159, 3252
IM3C	97, 100, 204, 231, 873, 1311, 1311, 1484, 1512, 1620, 2429, 2755, 3017, 3155, 3252
IM3D	53, 75, 142, 149, 909, 1308, 1308, 1485, 1511, 1633, 2408, 2777, 3053, 3159, 3251
TS6 (scrambling)	1034*i*, 32, 319, 326, 404, 687, 948, 1429, 1435, 2048, 2668, 3081, 3246, 3269, 3373
TS7 (S_N2, displacement)	1000*i*, 38, 521, 540, 744, 898, 1209, 1218, 1344, 1421, 1421, 3072, 3241, 3265, 3770
$CH_5^+ + H$	159, 905, 1308, 1311, 1486, 1511, 1632, 2408, 2772, 3049, 3158, 3250

[a] *i* stands for imaginary frequency.

TABLE 4: Harmonic Vibrational Frequencies at the CASSCF/AVTZ Level of Theory[a]

species	frequencies (cm^{-1})
$CH_4^+ + H_2$	783, 827, 1164, 1283, 1568, 2033, 2488, 3073, 3216, 4585
IM2	26, 408, 411, 605, 775, 832, 1104, 1149, 1419, 1419, 1522, 2944, 3113, 3115, 3693
TS2 (IM2 → IM3A)	584*i*, 137, 560, 560, 911, 1039, 1089, 1379, 1383, 1443, 1793, 1953, 2913, 3086, 3153
IM3B	73, 135, 264, 303, 949, 1292, 1316, 1476, 1493, 1599, 2199, 2778, 2966, 3052, 3135
TS6 (scrambling)	953*i*, 41, 316, 328, 390, 677, 927, 1421, 1424, 2114, 2632, 2964, 3127, 3142, 3285
$CH_5^+ + H$	232, 953, 1290, 1306, 1474, 1491, 1589, 2230, 2297, 2970, 3050, 3135

[a] *i* stands for imaginary frequency.

TABLE 5: Summary of the Calculated Reaction Enthalpy for the $CH_4^+ + H_2$ Reaction[a]

theory	CCSD	G3MP2	CCSD(T)-1	CCSD(T)-2	CF	MRCISD	Full CI
ΔE_e	−13.7	−13.9	−23.2	−24.3	−21.4	−21.2	−17.2
ΔZPE	9.8	9.8	9.8	9.1	9.1	8.9	8.9
ΔE_{rel}				0.1[b]			
ΔE_{DBOC}				−0.4[c]			
ΔE_{SO}				−0.1[d]			
ΔH^0	−4.3	−4.5	−13.8	−15.6	−12.7	−12.7	−8.6
ΔH^{298}	−6.1	−6.3	−15.6	−17.4	−14.5	−14.5	−10.4

[a] All numbers are in kJ/mol. The entries for theory: CCSD, CCSD/6-311++G(2d,2p) optimized geometries and ZPEs; G3MP2, G3MP2 procedure (ref 40) using the CCSD(full)/6-311++G(2d,2p) optimized geometries and ZPEs; CCSD(T)-1, RCCSD(T)/CBS(AVDZ, AVTZ, AVQZ extrapolation) using the CCSD(full)/6-311++G(2d,2p) optimized geometries and ZPEs; CCSD(T)-2, RCCSD(T)/CBS(AVQZ, AV5Z, AV6Z extrapolation using the RCCSD(T)/AVQZ optimized geometries and RCCSD(T)/AVTZ calculated ZPEs; CF, continued fractions approximation (ref 41) for the full CI energies using the RCCSD(T)/AV5Z energies with the RCCSD(T)/AVQZ optimized geometries and RCCSD(T)/AVTZ ZPEs; MRCISD, MRCISD/CBS(AVTZ, AVQZ, AV5Z extrapolation using the CASSCF/AVQZ optimized geometries and CASSCF/AVTZ calculated ZPEs; Full CI, MRCISD+Q/CBS(AVTZ, AVQZ, AV5Z extrapolation using the CASSCF/AVQZ optimized geometries and CASSCF/AVTZ calculated ZPEs. [b] ΔE_{rel} was calculated at the CISD/AVQZ // RCCSD(T)/AVQZ level of theory. CH_4^+: −38.8 kJ/mol. CH_5^+: −38.7 kJ/mol. [c] ΔE_{DBOC} was calculated at the CISD/VTZ // RCCSD(T)/AVQZ level of theory. CH_4^+: 6.7 kJ/mol. H_2: 1.4 kJ/mol. CH_5^+: 7.0 kJ/mol. H: 0.7 kJ/mol. [d] ΔE_{SO} was calculated at the CASSCF/AVTZ // RCCSD(T)/AVQZ level of theory. CH_4^+: 0.14 kJ/mol. CH_5^+: 0.09 kJ/mol.

TS6 represents the transition state for the scrambling mechanism. As shown in Figure 1, the H·H_2 group in IM2 moves away from CH_3 from 1.38 to 2.08 Å, forming a H_3 structure with three nearly equal HH bonds. Simultaneously, the H_3 structure rotates in the plane and flips over with one HH bond facing the C atom. The IRC calculation confirms that TS6 corresponds to the self-conversion of IM2, i.e., the scrambling transition state. Through the scrambling, one H atom can be exchanged between CH_4^+ and H_2. It is noted that the scrambling of IM2 does not produce anything new, but for the isotope reactions 2 and 3, the H−D scrambling produces $CH_3D^+ + H_2$ (reactions 2c) or $CH_3D^+ + HD$ (reaction 3b). The barrier height for TS6 is 47.9 kJ/mol, significantly higher than that for abstraction (TS2).

The last mechanism we found is an S_N2-type displacement via TS7. H_2 approaches CH_4^+ vertically, forming two new CH bonds simultaneously. The opposite H atom is kicked out to generate the final products CH_5^+ and an H atom (strictly speaking, the complex IM3D). A significant barrier exists for this process. The barrier height of 51.0 kJ/mol is even higher than that for the scrambling reaction.

In summary, the major reaction scheme can be shown as follows:

$$CH_4^+ + H_2 \rightarrow IM2 \rightarrow TS2 \rightarrow IM3 \rightarrow CH_5^+ + H$$

It corresponds to a "complex-forming" abstraction pathway. Neither scrambling nor S_N2 displacement can compete with the above mechanism. This conclusion is in agreement with the experimental results of ASSG. It was reported that there is no evidence for H−D scrambling in $CH_4^+ + HD/D_2$ collisions.[21]

The isotope reaction $CH_4^+ + D_2$ has the same mechanism as the $CH_4^+ + H_2$ reaction. The energy of TS2 increases to 3.2 kJ/mol above the reactants when D_2 is used as the reactant. It is interesting to note that the $CH_4^+ + HD$ involves one more mechanism, as shown in Figure 3. Starting from IM2 (strictly speaking, there are two IM2 isotopes, i.e., $H_3C{\cdot}H{\cdot}HD$ and $H_3C{\cdot}H{\cdot}DH$; however, these two structures are identical because the

internal rotation around C·H is free), there are two TS2 structures. One is the H atom connects to the C atom and the D atom moves away with the formation of $CH_5^+ + D$. The other is the D atom bonds to the C atom and the H atom moves away with the formation of $CH_4D^+ + H$. As can be seen in Figure 3, the $CH_5^+ + D$ channel is less exothermic than the $CH_4D^+ + H$ channel. However, the energies of the transition states (TS2) are almost identical (ca. 2.4 kJ/mol). The isotope substitution increases the net abstraction barriers slightly.

2. Comparisons between RCCSD(T) and CASSCF and MRCISD. Because the lowest potential energy surface (PES) for the title reaction is an open-shell doublet, CASSCF and MRCISD calculations for both geometries and energies were carried out to investigate the multiconfiguration characters of the reaction. Only the important species were studied. The structural parameters are shown in Figure 1c, and the energies are listed in Table 2. It is evident that the CASSCF/AVTZ optimized parameters are almost the same as the CASSCF/AVQZ data. In comparison with the CCSD/6-311++G(2d,2p) optimized geometries, the CASCF results do show some differences in both bond distances and angles. For example, even for the closed-shell CH_5^+, the two CH bonds in the 3-center CH_2 group are about 0.05 Å longer and the HH bond becomes 0.08 Å shorter. Interestingly, it appears that most of bonds in IM2, TS2, IM3, and TS6 tend to be longer at the CASSCF level. This comparison clearly shows that both dynamic and nondynamic electron correlations play important roles in the present system. Fortunately, the difference between CASSCF and CCSD results is not significant. As can be seen from Tables 1 and 2, the MRCISD/CBS energies are in general agreement with the RCCSD(T)/CBS data except for two points of significance. First, the barrier height for TS2 was calculated to be about 5 kJ/mol at the MRCISD/CBS level, about 3 kJ/mol higher than the RCCSD(T)/CBS value. Second, the MRCISD+Q level predicts smaller reaction exothermicity than MRCISD and RCCSD(T) (e.g., −8.2 kJ/mol vs −12.3 and −13.4 kJ/mol).

The average absolute deviation of 19 pairs of the relative energies presented in Tables 1 ($\Delta E_{G3MP2} - \Delta E_{RCCSD(T)/CBS}$) and 2 ($\Delta E_{MRCISD} - \Delta E_{Full-CI}$) is about 4 kJ/mol. Thus an error bar of ±4 kJ/mol is estimated for the calculated relative energies. The uncertainty in the RCCSD(T)/CBS calculation mainly comes from the absence of higher excitations such as CCSDTQ and the nondynamic correlation whereas that in MRCISD/CBS mainly comes from the incomplete reference configurations because only valence electrons and orbitals were considered. Therefore, an error bar of ±4 kJ/mol seems to be reasonable. At present, the barrier heights and heats of reaction are comparable with the magnitude of uncertainty. It is difficult to lower the errors further by either method.

For comparison, the vibrational frequencies are listed in Tables 3 (CCSD) and 4 (CASSCF). Most of frequencies are very close between the two levels of theory. Unfortunately, even for CH_4^+ and CH_5^+, there is no experimental vibrational data available for comparison. The very recent diffusion Monte Carlo calculation on CH_5^+ gives ZPE = 10 975 cm^{-1},[16] which agrees with our harmonic ZPE of 11 259 (CASSCF/AVTZ) and 11 475 cm^{-1} [CCSD/6-311++G(2d,2p)]. In addition, it is worth noting that the imaginary vibrational frequency of TS2 is −584 cm^{-1} at the CASSCF/AVTZ level, which is 168 cm^{-1} larger than the CCSD value. The magnitude of the imaginary frequency affects the significance of tunneling effect at low temperatures.

3. Kinetic Analysis. For simplicity, the simplified reaction scheme, e.g., $CH_4^+ + H_2 \leftrightarrow$ IM2 $\leftrightarrow$ TS2 $\leftrightarrow$ IM3B $\rightarrow CH_5^+ +$ H, was used in the calculation of rate coefficient. The temperatures range from 5 to 1000 K. It should be noted that the scrambling and displacement reactions can be competitive at higher temperatures. Only the low-pressure limit was considered currently; that is, the deactivation of IM2 and IM3 by collision is omitted. The collisionless radiative rates for the reaction intermediates were included, although their contribution to the overall rates is fairly small.

The bottlenecks of both entrance ($CH_4^+ + H_2 \rightarrow$ IM2) and exit channels (IM3B $\rightarrow CH_5^+ +$ H) were evaluated explicitly and variationally using flexible transition state theory[42] at the *E*/*J* resolved level.[43] The number of states of the transitional modes was calculated using the quantum phase-space theory[35] on the basis of the ion-induced-dipole potentials with the experimental polarizability of H_2 (0.8 $Å^3$) and H (0.67 $Å^3$). TS2 was treated using the rigid-rotor harmonic oscillator (RRHO) approximation. The tunneling coefficient was calculated using the one-dimensional Eckart potential.[44] The rotational partition functions were calculated by direct quantum counts. Moreover, a free internal rotator was used for IM2 to take account of the nearly free rotation of $H_3C{\cdot}H{\cdot}H_2$ around C·H bond.

Special attention has been paid for the symmetry numbers (σ) of reactants and products. Because we used explicitly ortho- and para-H_2 and thus $\sigma(H_2) = 1$, CH_4^+ has a C_{2v} structure with $\sigma = 2$. However, CH_4^+ is a fluxional ion and its geometry deviates from the parent T_d symmetry due to the Jahn−Teller effect. Thus we used $\sigma = 12$ instead of 2 for CH_4^+. As for CH_5^+, $\sigma = 5$ because of its five nearly equivalent CH bonds.

The rate coefficients are shown in Figure 4. The experimental data of ASSG[21] (solid circles) at 15−300 K are included in the figure for comparison. The energy-dependent rate coefficients obtained by Federer et al. are presented as well (open cirlces).[20] These nonthermal data were converted into an effective temperature *T* by using the simple relation $E_T = 1.5\ RT$.

The theoretical rate coefficients for the $CH_4^+ + H_2$ reaction are in good agreement with the experimental values in the range 20−100 K. Beyond this range, the calculated rate coefficients are generally higher than the experimental data. For example, at 300 K, the theoretical value is about twice the experimental value. The rate coefficients decrease rapidly as the temperature increases. However, above 300 K, the rate coefficients start to increase, in contrast to the experimental data of Federer et al.,[20] which still decrease with the evaluated temperature. It is very interesting to note that the theoretical and experimental rate coefficients in Figure 3 look just like two “) ” and “ (” brackets in the mirror.

Before we discuss the possible reasons for the discrepancy between theory and experiment, it is noted that the high-temperature rate coefficients themselves are suspicious in Figure 4 because of the well-known difficulties of comparing thermal rate coefficients with results from SIFDT experiments. Trajectory calculation is required to calculate the energy-dependent rate coefficients.

No matter how large the error bars for the experimental data (ca. 10%?), we point out three potential uncertainties in the theoretical rate coefficients. First, the reaction system itself might not be a statistical assembly but the statistical TST, RRKM, and PST methods were used to treat it. The number of states and density of states have been calculated at the specific *E* and *J* using the vibrational frequencies of the *global* minimum. The worst scenario is that the present kinetic simulation can be wrong quantitatively. However, this does not happen because the theoretical rate coefficients do show agreement with experimental data over a specific range of temperatures. Thus it can be argued that the title reaction may be treated statistically at

least in some regions. Second, the barrier height for TS2 is uncertain. As mentioned above, there are around 3 kJ/mol difference in the barrier between RCCSD(T) and MRCISD methods. Such a small difference has significant influence on the low-temperature rates. The high-temperature rates are seldom affected. As shown in Figure 4, if the MRCISD/CBS calculated energies and the CASSCF/AVTZ geometrical parameters and frequencies were used, the rate coefficients become much smaller, but the room-temperature rate becomes closer to the experimental result. Note that adjustment of the barrier height for TS2 cannot fit the whole set of experimental data. Third, the one-dimensional Eckart tunneling shows good performance for many chemical reactions. However, it might not be quantitatively good enough for the present system especially at low temperatures. It has been shown that the tunneling correction tends to be overestimated by the Eckart scheme at extremely low temperatures, in comparison with the more realistic multidimensional methods such as small-curvature tunneling (SCT).[45,46] The tunneling effect plays a critical role for the low-temperature rate coefficients. For example, at 10 K, the magnitude of the tunneling correction is as large as 10^{10}. As the temperature increases, the contribution of tunneling decreases dramatically. At 150 K, the tunneling correction is only a factor of 2. At 1000 K, the tunneling does not play a role.

The most important (qualitatively) characteristic of the theoretical rate coefficients is that there is a minimum around 300 K (or 100 K with the MRCISD+Q data). This is reasonable in the consideration of the fact that a barrier (TS2) exists along the reaction path. At higher temperatures, the tunneling effect plays less and less a role, and thus the reaction is mainly determined by the activation barrier. In addition, as can be seen in Figure 4, the ortho-H_2 reaction is faster than the para-H_2 reaction below 100 K. At higher temperatures, they have nearly equal rate coefficients.

The rate coefficients for the two isotope reactions 2 and 3 are shown in Figure 5. Evidently, a similar temperature dependence was obtained. For the $CH_4^+ + HD$ reaction, the overall rate coefficients are smaller than those for the $CH_4^+ + H_2$ reaction below 400 K. At higher temperatures, the former becomes a little larger. At 300 K, the rate coefficients are almost the same for the reactions of CH_4^+ with HD and H_2. Reaction of CH_4^+ with D_2 is much slower than with H_2 or HD, in agreement with the experimental observation. Meanwhile, the minima of rate coefficients move to around 100 and 60 K for $CH_4^+ + HD$ and $CH_4^+ + D_2$ reactions, respectively.

One of the interesting characters of the $CH_4^+ + HD$ reaction is that there are two product channels, leading to $CH_5^+ + D$ and $CH_4D^+ + H$, respectively. As can be seen from Figure 5, the $CH_5^+ + D$ channel always prevails over the $CH_4D^+ + H$ channel, as indicated by the larger rate coefficients for the former in the whole temperature range considered. The yield of CH_5^+ was shown in Figure 6 to compare with the experimental data. It can be seen that CH_5^+ is always the major product of reaction 2 with branching ratios greater than 50%, in good agreement with the experimental observation.[21] The calculated absolute yields of CH_5^+ are a little smaller than the experimental data by about 10%. Through the analysis of the structure of the rate-determining TS2, it is known that the rotation constants of TS2 for $CH_5^+ + D$ channel are smaller than those for $CH_4D^+ + H$ channel (e.g., 4.42/1.03/1.00 cm^{-1} versus 4.42/1.27/1.24 cm^{-1}). Moreover, TS2 for $CH_5^+ + D$ channel has a slightly larger imaginary frequency (385 cm^{-1}). The smaller rotational constants are, the larger the number of states is; the larger the imaginary frequencies are, the more significant tunneling effect is. Therefore, the contributions of both rotational levels and tunneling effect lead the $CH_5^+ + D$ channel a little more favorable than the $CH_4D^+ + H$ channel even though the latter is more preferable thermodynamically.

4. Thermochemistry. The exothermicity of the title reaction is of importance to understand the destruction process of CH_5^+ by H atom. Experimentally, it was found that the title reaction is thermoneutral ($\Delta H_r^0 \approx 0$).[13] Two earlier estimations were reported, $\Delta H_r^0 = -5$ kJ/mol based on the SIFDT study[20] and $\Delta H_r^0 = -19$ kJ/mol based on the enthalpies of formation.[22] The calculated ΔH_r^0 in this work were summarized in Table 5. In view of the electronic energies (ΔE_e), it is evident that RCCSD(T) predicts the consistent data with MRCISD, ranging from -21.2 to -24.3 kJ/mol. It is interesting to note that the Full CI estimation based on the MRCISD+Q energies gives slightly smaller ΔE_e than the MRCISD theory. CCSD and G3MP2 give the smallest values.

A few corrections were made to ΔE_e. The most significant correction is, of course, ZPE. The ZPE corrections (ΔZPE) were calculated at three levels of theory, namely, CCSD/6-311++G-(2d,2p), RCCSD(T)/ AVTZ, and CASSCF/AVTZ. The harmonic ZPE of H_2 molecule was calculated to be 2208, 2198, and 2292 cm^{-1}, respectively, which is in good agreement with the experimental value 2179 cm^{-1}. There are no experimental data for CH_4^+ and CH_5^+. It is noted that the calculated ZPE for CH_5^+ (e.g., 11 475, 11 382, and 11 259, respectively) is in agreement with the very recently DMC calculated 10957 cm^{-1}.[16] Therefore, the harmonic ZPE data were used to calculate ΔZPE without scaling. As shown in Table 2, ΔZPE are +9.8, +9.1, and +8.9 kJ/mol, respectively. An average value of +9.3 kJ/mol was obtained. An error bar of ± 2 kJ/mol was estimated for ΔZPE.

Molecular scalar relativistic corrections (ΔE_{SR}),[29] which account for changes in the relativistic contributions to the total energies of the molecule and the constituent atoms, were included at the CISD level of theory using AVQZ basis set in the frozen core approximation. ΔE_{SR} is taken as the sum of the mass−velocity and one-electron Darwin (MVD) terms in the Breit-Pauli Hamiltonian. It turns out that the ΔE_{SR} is only +0.1 kJ/mol, although the absolute value of E_{SR} of each species is quite large.

Corrections that are due to the Born−Oppenheimer approximation have also been included by calculating the diagonal correction (DBOC).[30] These calculations used the formulas as implemented in PSI at the CISD level with the cc-pVTZ basis set. A value of $\Delta E_{DBOC} = -0.4$ kJ/mol was obtained.

Finally, the spin−orbital correction has been estimated at the CASSCF/AVTZ level of theory using the implications in Gaussian03.[31] To compute the spin−orbit coupling, the integrals were computed in a one-electron approximation involving relativistic terms, and then effective charges were used that scale the Z value for each atom to empirically account for 2-electron effects. It was found that $\Delta E_{SO} = -0.1$ kJ/mol.

With the above corrections, the predicted ΔH_r^0 data are listed in Table 5. ΔH_r^0 is only -4.3 and -4.5 kJ/mol at the CCSD and G3MP2 levels. Although both values appear to be in best agreement with the experimentally preferable thermoneutral result, it is known that both levels of theory result in large error bars (e.g., $\pm$ 8 kJ/mol). The RCCSD(T) and MRCISD levels of theory predict very similar ΔH_r^0, ranging from -12.7 to -15.6 kJ/mol. However, ΔH_r^0 with the estimated Full CI is about 4 kJ/mol smaller. We took the average value of the RCCSD(T), MRCISD, and Full CI calculated data as our best estimation: $\Delta H_r^0 = -12.7 \pm 5.2$ kJ/mol (2σ standard error).

At 298 K, $\Delta H_r^0 = -13.5 \pm 5.2$ kJ/mol. It is interesting to note that our best estimation is by coincidence in the middle of previous data (e.g., 0 to −19 kJ/mol).

The straightforward conclusion drawn from the present ΔH_r^0 value is that the reverse reaction, $CH_5^+ + H \rightarrow CH_4^+ + H_2$, should be much slower than the title reaction, which is in conflict with the experiments.[20,21] At room temperature the destruction of CH_5^+ by H atom was observed to be 10 times faster than its production via the $CH_4^+ + H_2$ reaction. Neither ab initio nor kinetic data support the experimental results of Federer et al. It is impossible to understand such a discrepancy so far. Two possibilities are suggested. First, the reaction in the SIFDT experiment of Federer et al. is not a thermalized system and cannot compare with our statistical results directly. Second, other unknown mechanism might exist for the $CH_5^+ + H$ reaction.

IV. Concluding Remarks

This computational work reveals that the $CH_4^+ + H_2$ reaction occurs via three mechanisms: complex-forming abstraction, scrambling, and S_N2 displacement. The last two mechanisms have contributions only at high temperature because of the significant barrier involved. The abstraction reaction proceeds via a very minor net barrier.

A few CH_6^+-like wells exist on the PES. The well on the reactant side, IM2, is a key intermediate. It is a very floppy $H_3C{\cdot}H{\cdot}H_2$ structure but not a fluxional ion. The CH_3 and H_2 groups can rotate freely around the central long C·H bond. The wells on the product side are a series of weakly bound $CH_5^+{\cdot}H$ complexes. The H atom runs in a circular orbital around CH_5^+ and thus these complexes are fluxional.

The rate coefficients show negative temperature dependence below 300 K and positive dependence at higher temperatures. The good agreement between theory and experiment has been obtained for the medium temperatures (20−100 K). At lower or higher temperatures, a large discrepancy exists. Nuclear spin plays a role at low temperatures. CH_4^+ reacts with ortho-H_2 much faster than with para-H_2. However, at temperatures above 300 K, both ortho- and para-H_2 have the same rate coefficients.

The $CH_4^+ + H_2$ reaction shows a significant isotope effect. For the $CH_4^+ + HD$ reaction, two product channels exist, forming $CH_5^+ + D$ and $CH_4D^+ + H_2$, respectively. The less exothermic $CH_5^+ + D$ channel prevails over the $CH_4D^+ + H_2$ channel in the range 5−1000 K, in agreement with the experiments. For the $CH_4^+ + D_2$ reaction, the rate coefficients are smaller than those of the reactions of CH_4^+ with H_2 and HD. Moreover, the minima of the rate coefficients are at 100 and 60 K for $CH_4^+ + HD$ and D_2 reactions.

The best estimated heat of reaction for the $CH_4^+ + H_2 \rightarrow CH_5^+ + H$ reaction is $\Delta H_r^0 = -12.7 \pm 5.2$ kJ/mol at 0 K, indicating that the title reaction is exothermic.

Acknowledgment. This work was supported by A Foundation for the Author of National Excellent Doctoral Dissertation of PR China (FANEDD, 200224) and by the Scientific Research Foundation for the Returned Overseas Chinese Scholars, State Education Ministry. We thank Prof. Dr. D. Gerlich (Technische Universitaet Chemnitz) for helpful discussions.

References and Notes

(1) Eriksson, L. A.; Lunell, S. B.; Russell J. *J. Am. Chem. Soc.* **1993**, *115*, 6896.
(2) Paddon-Row: M. N.; Fox, D. J.; Pople, J. A.; Houk, K. N.; Pratt, David W. *J. Am. Chem. Soc.* **1985**, *107*, 7696.
(3) Frey, R. F.; Davidson, E. R. *J. Chem. Phys.* **1988**, *88*, 1775.
(4) Ohta, Y.; Ohta, K. *J. Comput. Chem.* **2004**, *25*, 1910.
(5) Rasul, G.; Prakash, G. K. S.; Olah, G. A. *Proc. Natl. Acad. Sci. USA* **1997**, *94*, 11159.
(6) Signorell, R.; Sommavilla, M. *J. Electron. Spectrosc. Relat. Phenom.* **2000**, *108*, 169.
(7) Thompson, K. C.; Crittenden, D. L.; Jordan, M. J. T. *J. Am. Chem. Soc.* **2005**, *127*, 4954.
(8) Marx, D.; Parrinello, M. *Nature* **1995**, *375*, 216.
(9) Vager, Z.; Kanter, E. P.; Both, G.; Cooney, P. J.; Faibis, A.; Koenig, W.; Zabransky, B. J.; Zajfman, D. *Phys. Rev. Lett.* **1986**, *57*, 2793.
(10) White, E. T.; Tang, J.; Oka, T. *Science* **1999**, *284*, 135.
(11) Marx, D.; Parrinello, M. *Science* **1999**, *284*, 59.
(12) Schreiner, P. R. *Angew. Chem., Int. Ed.* 18, Wiley-VCH Verlag: **2000**, *39*, 3239.
(13) Gerlich, D. *Phys. Chem. Chem. Phys.* **2005**, *7*, 1583.
(14) Kaledin, A. L.; Kunikeev, S. D.; Taylor, H. S. *J. Phys. Chem. A* **2004**, *108*, 4995.
(15) Muller, H.; Kutzelnigg, W.; Noga, J.; Klopper, W. *J. Chem. Phys.* **1997**, *106*, 1863.
(16) Brown, A.; McCoy, B.; Braams, B. J.; Jin, Z.; Bowman, J. M. *J. Chem. Phys.* **2004**, *121*, 4105.
(17) Munson, M. S. B.; Field, F. H.; Franklin, J. L. *J. Am. Chem. Soc.* **1963**, *85*, 3584.
(18) Kim, J. K.; Thread, L. P.; Huntress, W. T., Jr. *J. Chem. Phys.* **1975**, *62*, 45.
(19) Adams, N. G.; Smith, D. *Chem. Phys. Lett.* **1977**, *47*, 383.
(20) Federer, W.; Villingen, H.; Tosi, P.; Bassi, D.; Fergusson, E.; Lindinger, W. In *Molecular Astrophysics − State of the Art and Future Directions*; Diercksen, G. H. F., et al., Eds.; Reidel: Boston, 1985; p 649.
(21) Asvany, O.; Savic, I.; Schlemmer, S.; Gerlich, D. *Chem. Phys.* **2004**, *298*, 97.
(22) Le Teuff, Y. H.; Millar, T. J.; Marwick, A. J. *Astron. Astrophys. Sippl. Ser.* **2000**, *146*, 157.
(23) (a) Purvis, G. D., III.; Bartlett, R. J. *J. Chem. Phys.* **1982**, *76*, 1910. (b) Raghavachari, K.; Trucks, G. W.; Pople, J. A.; Head-Gordon, M. *Chem. Phys. Lett.* **1989**, *157*, 479. (c) Watts, J. D.; Gauss, J.; Bartlett, R. J. *J. Chem. Phys.* **1993**, *98*, 8718.
(24) (a) Hampel, C.; Peterson, K. A.; Werner, H. J. *Chem. Phys. Lett.* **1990**, *190*, 1. (b) Deegan, M. J. O.; Knowles, P. J. *Chem. Phys. Lett.* **1994**, *227*, 321. (c) Knowles, P. J.; Hampel, C.; Werner, H. J. *J. Chem. Phys.* **1988**, *99*, 5219.
(25) Dunning, T. H. *J. Chem. Phys.* **1989**, *90*, 1007.
(26) Feller, D. *J. Chem. Phys.* **1992**, *96*, 6104.
(27) Huh, S. B.; Lee, J. S. *J. Chem. Phys.* **2003**, *118*, 3035.
(28) Gonzalez, C.; Schlegel, H. B. *J. Chem. Phys.* **1989**, *90*, 2154. (b) Gonzalez, C.; Schlegel, H. B. *J. Phys. Chem.* **1990**, *94*, 5523.
(29) (a) Cowan, R. D.; Grin, M. J. *Opt. Soc. Am.* **1976**, *66*, 1010. (b) Martin, R. L. *J. Phys. Chem.* **1983**, *87*, 750. (c) Davidson, E. R.; Ishikawa, Y.; Malli, G. L. *Chem. Phys. Lett.* **1981**, *84*, 226.
(30) (a) Handy, N. C.; Yamaguchi, Y.; Schaefer, H. F. *J. Chem. Phys.* **1986**, *84*, 4481. (b) Schwenke, D. W. *J. Phys. Chem. A* **2001**, *105*, 2352. (c) Valeev, E. F.; Sherrill, C. D. *J. Chem. Phys.* **2003**, *118*, 3921.
(31) Abegg, P. W. *Mol. Phys.* **1975**, *30*, 579.
(32) (a) Werner, H.-J.; Knowles, P. J. *J. Chem. Phys.* **1988**, *89*, 5803. (b) Knowles, P. J.; Werner, H.-J. *Chem. Phys. Lett.* **1988**, *145*, 514.
(33) (a) Werner, H.-J.; Knowles, P. J. *J. Chem. Phys.* **1985**, *82*, 5053. (b) Knowles, P. J.; Werner, H.-J. *Chem. Phys. Lett.* **1985**, *115*, 259.
(34) Helgaker, T.; Klopper, W.; Koch, H.; Noga, J. *J. Chem. Phys.* **1997**, *106*, 9639.
(35) (a) Pechukas, P.; Light, J. C. *J. Chem. Phys.* **1965**, *42*, 3281. (b) Pechukas, P.; Rankin, R.; Light, J. C. *J. Chem. Phys.* **1966**, *44*, 794.
(36) Frisch, M. J.; et al. *Gaussian 03*, Revision B.05; Gaussian, Inc.: Pittsburgh, PA, 2003.
(37) Werner, H.-J.; et al. MOLPRO, version 2002.6.
(38) Crawford, T. D.; et al. PSI 3.2, 2003.
(39) Klippenstein, S. J.; et al. VARIFLEX: version1.00, 1999.
(40) Curtiss, L. A.; Redfern, P. C.; Raghavachari, K.; Rassolov, V.; Pople, J. A. *J. Chem. Phys.* **1999**, *110*, 4703.
(41) Goodson, D. Z. *J. Chem. Phys.* **2002**, *116*, 6948.
(42) Wardlaw, D. M.; Marcus, R. A. *Chem. Phys. Lett.* **1984**, *110*, 230.
(43) Klippenstein, S. J. *J. Phys. Chem.* **1994**, *98*, 11459.
(44) Miller, W. H. *J. Am. Chem. Soc.* **1979**, *101*, 6810.
(45) Truong, T. N. *J. Phys. Chem. B* **1997**, *101*, 2750.
(46) Truhlar, D. G.; Isaacson, A. D.; Skodje, R. T.; Garrett, B. C. *J. Phys. Chem.* **1982**, *86*, 2252.
(47) Herzberg, G.; Monfils, A. *J. Mol. Spectrosc.* **1960**, *5*, 482.